Ann. Geophys., 27, 3755–3764, 2009
www.ann-geophys.net/27/3755/2009/

Annales Geophysicae

On the SuperDARN cross polar cap potential saturation effect

A. V. Koustov[1], **G. Ya. Khachikjan**[1,*], **R. A. Makarevich**[2], **and C. Bryant**[1]

[1]Institute of Space and Atmospheric Studies, University of Saskatchewan, 116 Science Place, Saskatoon, Saskatchewan, S7N 5E2 Canada
[2]Department of Physics, La Trobe University, Melbourne, Victoria, 3086, Australia
[*]on leave from: Institute of Seismology, al-Farabi, 75a, 050060, Almaty, Kazakhstan

Received: 2 November 2008 – Revised: 20 August 2009 – Accepted: 17 September 2009 – Published: 5 October 2009

Abstract. Variation of the cross polar cap potential (CPCP) with the interplanetary electric field (IEF), the merging electric field E_{KL}, the Polar Cap North (PCN) magnetic index, and the solar wind-magnetosphere coupling function E_C of Newell et al. (2007) is investigated by considering convection data collected by the Super Dual Auroral Radar Network (SuperDARN) in the Northern Hemisphere. Winter and summer observations are considered separately. All variations considered show close to linear trend at small values of the parameters and tendency for the saturation at large values. The threshold values starting from which the non-linearity was evident were estimated to be IEF*$\sim E^*_{KL}\sim$3 mV/m, PCN*$\sim$3–4, and $E^*_C\sim 1.5\times10^4$. The data indicate that saturation starts at larger values of the above parameters and reaches larger (up to 10 kV) saturation levels during summer. Conclusions are supported by a limited data set of simultaneous SuperDARN observations in the Northern (summer) and Southern (winter) Hemispheres. It is argued that the SuperDARN CPCP saturation levels and the thresholds for the non-linearity to be seen are affected by the method of the CPCP estimates.

Keywords. Ionosphere (Electric fields and currents) – Magnetospheric physics (Magnetosphere-ionosphere interactions; Solar wind-magnetosphere interactions)

1 Introduction

Observations show that the ionospheric cross polar cap potential (CPCP) tends to saturate at extreme solar wind conditions (e.g., Siscoe et al., 2004; Shepherd, 2007). The effect has been demonstrated by considering $\boldsymbol{E}\times\boldsymbol{B}$ ion drift data from satellites crossing the polar cap (e.g., Hairston et al., 2003), by modeling the CPCP with AMIE technique based on magnetometer data (e.g., Russell et al., 2001; Liemohn and Ridley, 2002) and by analyzing the SuperDARN radar convection maps (e.g., Shepherd et al., 2003; Khachikjan et al., 2008). To show the saturation effect, the CPCP has been plotted against either the interplanetary electric field (IEF, Russell et al., 2001; Khachikjan et al., 2008) or the merging electric field E_{KL} (Shepherd et al., 2003). While the first consideration characterizes the ionospheric output (CPCP) and the external driver (IEF), the second consideration takes into account the relationship between the external driver and the magnetosphere/ionosphere system. SuperDARN data seem to show the saturation effect in a more profound way than the other instruments.

Ridley and Kihn (2004) investigated the AMIE-modeled CPCP variation with the polar cap magnetic index. The polar cap index (e.g., Troshichev et al., 2006) is derived from magnetometer records at a single polar cap station. For the Northern Hemisphere, data from the Thule magnetometer are used, and the index is called the PCN index. For the Southern Hemisphere, Vostok magnetometer data are considered and this index is called the PCS index. In the process of polar cap indices calculation, measured magnetic perturbations are correlated with the merging electric field E_{KL} so that the indices ultimately reflect the merging electric field E_{KL} but they are not exactly equivalent to it. Ridley and Kihn (2004) demonstrated little nonlinearity in the CPCP-PCN relationship, although they considered only moderately disturbed conditions (PCN$<$3–4). This finding is consistent with the almost linear relationship between AMIE-based CPCP and IEF in a range between 0 and 10 mV/m (Liemohn and Ridley, 2002).

Thus, published data show that the character of the CPCP increase with IEF, E_{KL}, or PCN and the saturation level (if it exists) depend on the method of the CPCP measurements/estimates and the selection of independent parameter. Notably, the threshold value for the nonlinearity to begin and

Correspondence to: A. V. Koustov
(sasha.koustov@usask.ca)

Published by Copernicus Publications on behalf of the European Geosciences Union.

the CPCP plateau values vary significantly (Liemohn and Ridley, 2002; Khachikjan et al., 2008).

A number of physical processes leading to the CPCP saturation have been discussed (e.g., Siscoe et al., 2004; Shepherd, 2007), but attempts to identify the dominating mechanism and the relative role of others have not been successful. Accumulation of experimental data on the CPCP as a function of various parameters characterizing the electrodynamics of the near Earth space is an urgent task. In pursuing this goal, useful information can be inferred from plotting the CPCP against other parameters. In terms of indices, an interesting relationship to consider is the CPCP versus the PCN index because the work by Ridley and Kihn (2004) did not show strong nonlinearity, which is in contrast with, for example, SuperDARN-based studies (Shepherd et al., 2003; Khachikjan et al., 2008). In terms of a function characterizing interaction of the solar wind and the magnetosphere, an interesting relationship to consider is the CPCP with the recently introduced by Newell et al. (2007) coupling function E_C. The E_C is a function showing best correlation with nine indices/parameters that are widely used in space physics.

This study is aimed at further investigation of the CPCP saturation effect. We consider CPCPs inferred from SuperDARN HF radar convection measurements and involve the PCN index and E_C function. The thrust of the study is on the character of the CPCP relationship upon these parameters and seasonal change in its character.

2 Data selection

We consider 2-min CPCPs inferred from SuperDARN convection measurements by applying the map potential technique of Ruohoniemi and Baker (1998). This method is deemed to be reliable, first of all, if significant amount of vectors is available for the analysis of an individual convection map. Maps that we considered had at least 200 points and, for the vast majority of cases (91% winter and 70% summer time), had more than 300 points (this threshold value was adopted by Khachikjan et al. (2008) whose events have mostly been included into the present data set). Since we wanted to consider the PCN magnetic index, the data search was limited to the periods for which the PCN index was visibly showing enhancements to 5–6 and up according to the plots on the official WEB site for PCN: http://web.dmi.dk/projects/wdcc1/pcn/pcn.html. We note that large PCNs are not that unusual, but, frequently, the SuperDARN coverage is poor to have a reliable CPCP estimate. In addition, we considered only those maps for which the radar measurements were available for both evening and morning convection foci areas. Certainly, this last criterion is somewhat subjective, but is important for selection of reliable CPCP measurements. Application of this criterion has led to a significant drop in a number of available maps. Despite the fact that three years of the SuperDARN network operation were searched, 2000–2002, only ∼1400 CPCP measurements were found for winter (November–February) and ∼1700 CPCP measurements for summer (May–July). The PCN values were downloaded from the above mentioned WEB site. Since we considered 2-min SuperDARN convection maps, the corresponding IEF, E_{KL}, PCN and E_C values were obtained by averaging over the corresponding 2-min intervals.

For producing the SuperDARN convection maps and CPCP estimates, the IMF parameters were obtained from the ACE magnetometer instrument and the delay time of the ACE measurements was determined according to Weimer et al. (2003). For the data set selected, the PCN was as high as 10 but for the majority of the CPCP data, the index was below 6 (summer) and 8 (winter).

3 CPCP as a function of IEF

We first plot the SuperDARN CPCP versus the IEF, Fig. 1. Khachikjan et al. (2008) investigated this relationship in detail, but with the data collected during predominantly winter time. We have two objectives: first, we would like to confirm that the SuperDARN data selected with somewhat different and more restrictive criteria still show the same tendencies and, second, we go further and consider the data for winter and summer separately. We note that although SuperDARN coverage is generally better for winter (e.g., Koustov et al., 2004), we selected as many events as possible for summer observations to have comparable winter and summer data sets.

Figure 1a (1b) is a scatter plot of the CPCP versus the IEF for summer (winter). A quick inspection tells us that, while the summer cloud of points is well-stretched in one direction, thus hinting on the close-to-linear dependence, the winter cloud of points seems to show stretching along one line for IEFs between −2 and ∼3 mV/m only. For IEF>∼5 mV/m, the CPCPs are clustered around the constant value of ∼80 kV so that the cloud of points seems to be "bent" at IEF∼3–5 mV/m and one can say that there is a saturation of the CPCP at large IEFs. To illustrate this tendency more clearly, we binned the CPCP data according to 1-mV/m bins of the IEF. Thick black line in Fig. 1 connects the obtained binned values of the CPCP. One can see the saturation effect at large IEFs for winter. It is less pronounced for summer. We comment that the summer data in Fig. 1a are somewhat inconclusive with respect to the saturation effect because the number of points for IEF>5 mV/m is not significant.

We also present in Fig. 1a, b a linear dependence inferred by Liemohn and Ridley (2002) from AMIE modeling (green line). For summer, the line is close to the binned CPCPs (black ragged line). For winter, a clear deviation of the SuperDARN CPCP from the AMIE linear trend is evident at large IEFs, starting from ∼3 mV/m. Similar diversion of AMIE and SuperDARN CPCPs was reported by Khachikjan

Table 1. Parameters of the linear fit line CPCP=$A+B\cdot X$.

	X	A, kV	B, kV/(X)	Corr. coeff.	St Dev, kV
L&R (2002)	PCN	58.10	7.29	–	–
SD, summer	IEF	(55.03) 52.36	(6.26) 8.14	(0.64) 0.46	(13.22) 12.68
SD, winter	IEF	(59.64) 50.66	(3.65) 11.27	(0.57) 0.58	(14.20) 13.00
SD, K(2008)	IEF	(50.18) 40.5	(3.60) 9.5	(0.52) 0.51	(15.06) 12.5
SD, summer	E_{KL}	38.80	12.27	0.70	10.59
SD, winter	E_{KL}	41.42	10.32	0.51	13.80
SD, summer	PCN	34.91	14.04	0.62	12.77
SD, winter	PCN	33.00	13.38	0.68	11.43
SD, summer	E_C	41.17	28.03	0.67	11.66
SD, winter	E_C	39.90	29.47	0.69	11.99

et al. (2008) whose data were heavily dominated by winter measurements.

To assess the CPCP-IEF relationship in more quantitative way, we considered three different fits to the data, Fig. 1c, d. First, we simply applied the linear fit (black line), similar to Liemohn and Ridley (2002). Table 1 presents the coefficients of these linear fits, placed in brackets. We also applied linear fitting to the data by Khachikjan et al. (2008) by considering their entire data set (in contrast to a limited IEF range in that study). One can conclude that for summer, the SuperDARN data are consistent with the AMIE results. For winter, the slope of the fit line is almost 2 times lower in a case of SuperDARN, both for our limited data set and for the one of Khachikjan et al. (2008). It is not a surprise that the correlation coefficient and the standard deviation from the best-fit linear line are better for summer observations.

One may argue that fitting a straight line to the cloud of points with obvious non-linear trend (winter data) is not very good way of assessing the data. Moreover, as will be discussed later, the SuperDARN measurements at large IEFs may be somewhat erroneous. For these reasons, we assessed only the linear part of the data in Fig. 1a, b by applying straight line fitting. Parameters of such fit depend on the IEF range that corresponds to the linear part of the trend. We adopted the threshold from which the nonlinearity kicks in as 3 mV/m, similar to Khachikjan et al. (2008). Parameters of these fits are also shown in Table 1, and the corresponding lines are shown in Fig. 1b by blue color. Clearly, the linear fits to the increasing part of the plots are much closer to the AMIE expectations. Also, there is not much of a difference (for the slope) between summer and winter data. In the analysis to follow, we applied linear fits to only growing part of each plot and plotted all lines by the same blue color.

Secondly, we performed the sigmoidal-Boltzman fitting of the same data, primarily for a comparison with the Khachikjan et al. (2008) results. In this approach, the following function was used: CPCP=$(A_1-A_2)/(1+\exp[(\mathrm{IEF}-x_0)/\Delta x])+A_2$, where the parameters A_1, A_2, x_0, and Δx were found by fitting procedure. We note that, generally, A_2 reflects the saturated CPCP value at large IEFs, Δx reflects the rate of reaching this saturation level, and x_0 characterizes the IEF value for the saturation to begin. Parameters of the Boltzman fit for our data set and the one of Khachikjan et al. (2008) are presented in Table 2 and the corresponding curves are shown in Fig. 1c, d by green color.

Again, one notices that parameters of the fits for our winter data are quite consistent with the ones by Khachikjan et al. (2008). The summer fit parameters are somewhat different; all three parameters A_2, Δx and x_0 are larger here. This means that the summer data show larger CPCP saturation level, this level is reached more slowly and the saturation begins at larger IEFs. These conclusions are consistent with the observation of the binned CPCPs in Fig. 1c, d.

Finally, we performed least-square fitting by applying the asymptotic exponential function used, for example, by Liemohn and Ridley (2002): CPCP(x)=$P-S\exp(-(x/T)$. The results of fitting are shown as red curves in Fig. 1c, d. We feel that this kind of function is reasonably suited for assessing our data because the shape of the obtained curve follows the data trends in Fig. 1 quite well. Parameter P tells us about the saturated level of the function at large values of the argument. Parameter T describes how fast the saturation level is achieved.

Inferred parameters of the exponential fit for our data and the ones of Khachikjan et al. (2008) are presented in Table 3 (columns 3–5) where we also give values for one of the exponential fits reported by Liemohn and Ridley (2002), first row. Winter data seem to be consistent for all three comparisons. For summer, the fit parameters for SuperDARN are very different from others and indicate that the relationship is much closer to a linear one, consistent with our conclusion from other types of fitting. This is especially evident if one realizes that parameter T is very large for the summer data. Parameter P is larger for summer measurements indicating higher level of the CPCP saturation for this season.

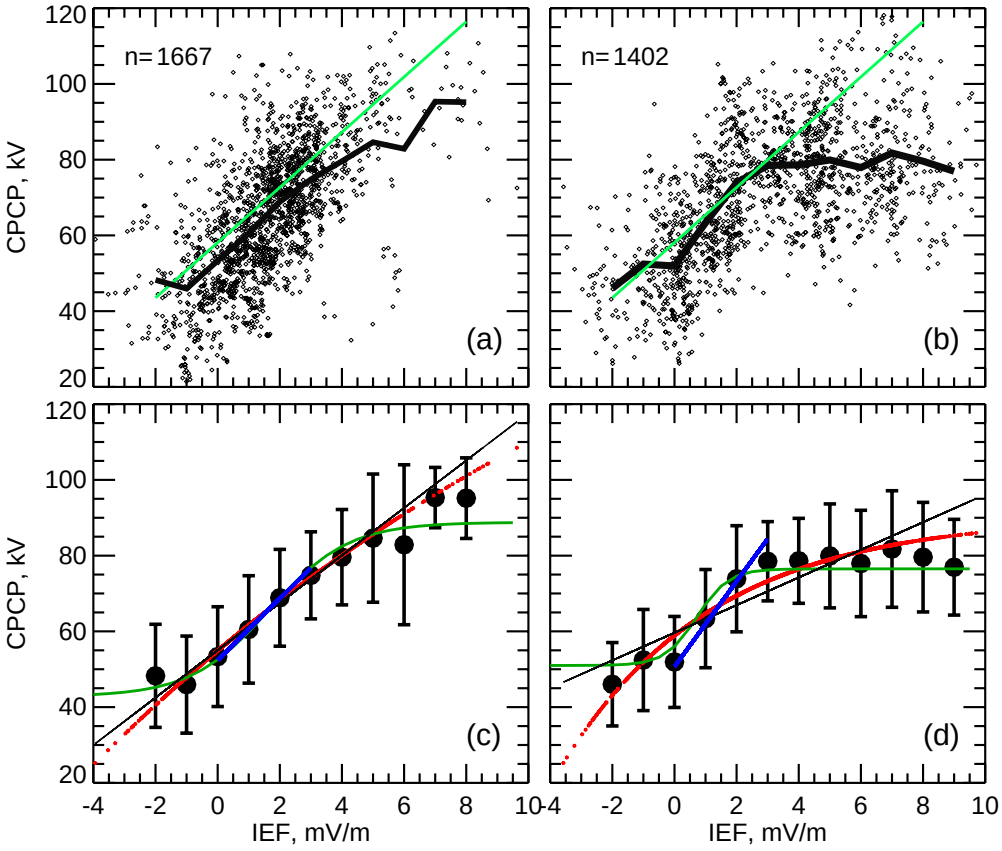

Fig. 1. Scatter plot of the cross polar cap potential (CPCP) inferred from SuperDARN radar measurements versus the interplanetary electric field (IEF) for **(a)** summer and **(b)** winter. Overlaid black thick lines connect the CPCP average values for IEF bins of 1-mV/m wide. The light green line is the linear relationship inferred by Liemohn and Ridley (2002) by using AMIE modeling. Panels **(c)** and **(d)** show various curves assessing the data of panels (a) and (b). Three different least square fits are considered: linear (black for the entire range of the IEF and blue for only growing part of the scatter plot), exponential (red) and sigmoidal-Boltzmann (dark green). The bin-averaged CPCPs (from panels a and b, respectively) and the corresponding standard deviations are also presented.

Table 2. Parameters of the Boltzman fit CPCP=$(A_1-A_2)/(1+\exp[(\mathrm{IEF}-x_0)/\Delta x])+A_2$.

	A_1, kV	A_2, kV	x_0, mV/m	Δx, mV/m	Corr. coeff.	St Dev, kV
Kh (2008)	40.8	73.3	1.32	0.69	0.65	13.43
Summer	42.8	88.8	1.67	1.27	0.66	12.95
Winter	53.4	79.5	1.3	0.43	0.59	13.89

4 CPCP as a function of E_{KL}, PCN and E_C

Now we sort the data according to the E_{KL}, PCN magnetic index and E_C function. Results are presented in Fig. 2 in the same format as in Fig. 1a, b, i.e. by showing the original points and the binned values of the CPCP.

Similar to Fig. 1 data, scatter plots of the CPCP versus E_{KL} and PCN, Fig. 2a, c and 2b, d (summer and winter, respectively) show an increasing part and saturation. The tendencies are more obvious if one considers binned values of the CPCP. The curves for both seasons show a somewhat more linear initial part at low values of parameters and a tendency to saturate at large values. Unfortunately, the summer data are limited to $E_{KL}\sim$6 mV/m and PCN ~4.5 and the saturation level cannot be inferred/estimated confidently. Winter data show the saturation effect quite clearly. To assess these dependencies, we performed linear fitting to the growing trend at small values of a respective parameter (obtained fit parameters are reported in Table 1) and asymptotic exponential fitting (red lines, obtained fit parameters are reported

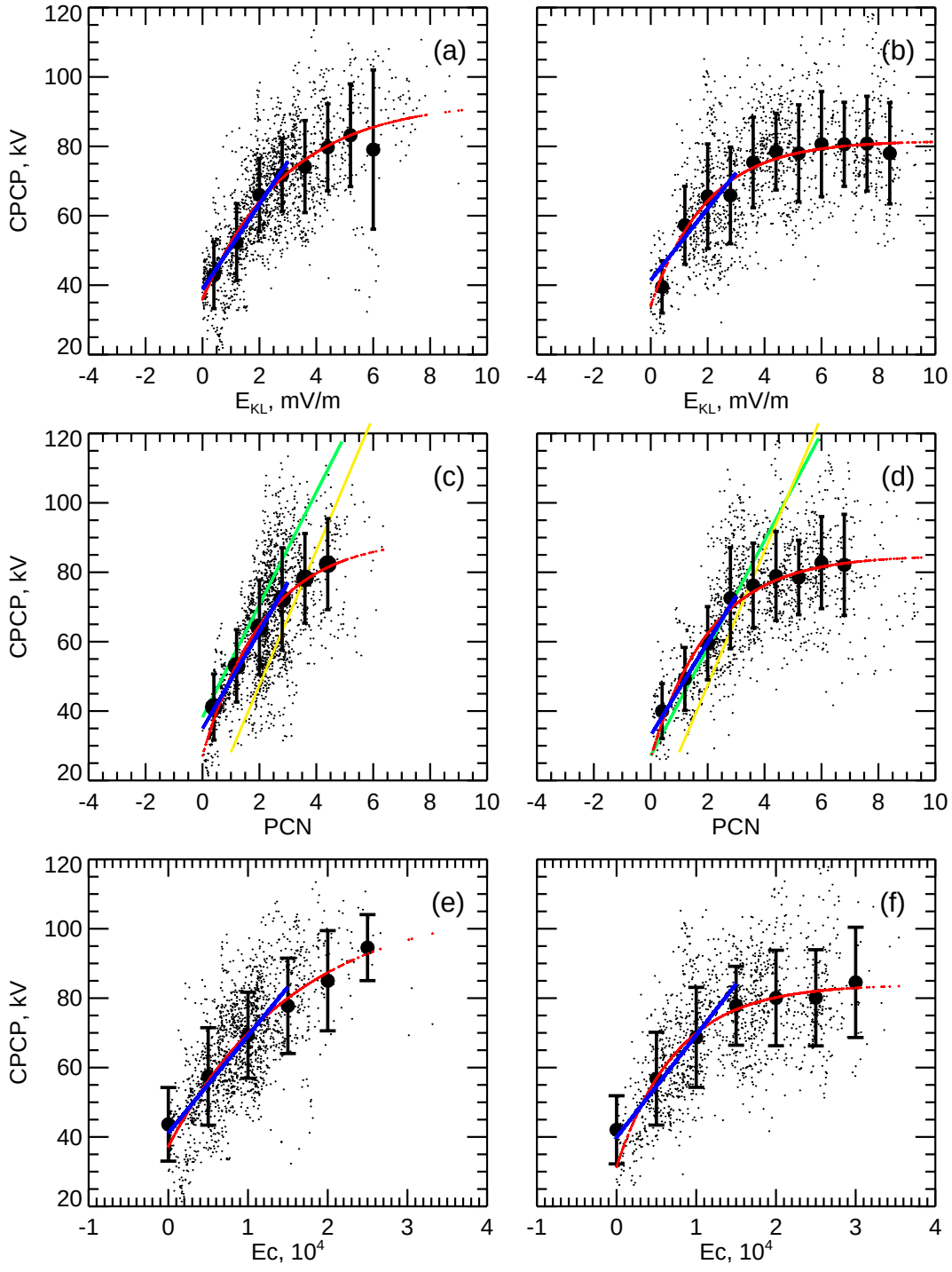

Fig. 2. **(a)** Scatter plot of the SuperDARN cross polar cap potential (CPCP) versus the E_{KL} function for summer measurements. Also presented are the CPCP binned values (solid dots, 0.5 mV/m step) and standard deviation for each bin. **(c)** The same as in (a) but versus the PCN magnetic index. The PCN bins are 0.5 units apart. The green line is the linear relationship obtained by Ridley and Kihn (2004) through AMIE modeling. The yellow line is the linear relationship reported by Troshichev et al. (1996). **(e)** The same as in (a) but for the Newell coupling function Ec. The bin width is 0.5×10^4. Panels **(b)**, **(d)**, and **(f)** are the same as (a), (c), and (e), respectively, but for winter measurements. In all panels, overlaid red line is the exponential least square fit to original (non-binned) data and overlaid blue line is the linear fits to the increasing part of the plots. Parameters of the fits are given in Tables 3 and 1, respectively.

Table 3. Parameters of the asymptotic exponential fit CPCP(x)=$P-S\exp(-(x/T)$.

	Parameter X	P, kV	S, kV	T, mV/m	SD, kV
AMIE, L-02	IEF	166.2	134.8	4.43	–
SD, Kh-08	IEF	94.15	45.98	6.16	–
SD, summer	IEF	205.38	150.50	21.88	13.19
SD, winter	IEF	90.31	31.43	4.91	13.67
SD, summer	E_{KL}	93.06	57.11	2.96	11.72
SD, winter	E_{KL}	81.59	47.52	1.98	13.39
SD, summer	PCN	90.04	62.94	2.21	13.03
SD, winter	PCN	84.86	58.35	2.20	12.54
SD, summer	E_C	107.40	70.13	1.60	11.87
SD, winter	E_C	83.93	52.45	0.76	12.63

in Table 3) to characterize an overall nonlinearity of a dependence.

While doing the linear fitting, thresholds for the linear parts of the dependencies were selected as E_{KL}=3 mV/m (consistent with Bristow et al., 2004) and PCN=3 (consistent with Khachikjan et al., 2008; Fiori et al., 2009). Obtained slopes of the straight lines (see blue lines in Fig. 2) are somewhat larger for the PCN dependence as compared to the E_{KL} dependence. For both parameters, the slopes are larger than for the CPCP dependence upon IEF. There is some difference of inferred parameters between seasons but no clear pattern can be inferred.

We note that the binned CPCPs for various E_{KL} in Fig. 2a, b are very close to the typical values reported by Shepherd et al. (2003) up to ∼3 mV/m. For E_{KL}>3 mV/m our values are slightly larger (maximum by ∼8 kV for E_{KL}∼5 mV/m). In Fig. 2c, d we also show the linear dependencies reported by Troshichev et al. (1996), satellite estimates of the CPCP (yellow line), and by Ridley and Kihn (2004), AMIE modeling (green line). Both summer and winter SuperDARN data are consistent with AMIE results for PCN between 0 and ∼3 and visual diversion of the data occurs starting from PCN ∼4. The line of Troshichev et al. (1996), which was obtained without considering the seasonal effect, have comparable slope but shifted down by ∼20 kV.

Figure 2e and 2f shows variation of the CPCP with E_C for summer and winter, respectively, in the same format as the data in Fig. 2a–d. Inferred parameters of the linear and exponential fits are given in Tables 1 and 3, respectively. The range of the E_C is comparable here for the two seasons and one can recognize much more nonlinearity in the relationship for winter measurements. This conclusion is consistent with larger T-value for the summer data. Similar to inference from other fits, the saturated CPCP is larger for the summer data set. It is interesting that sorting CPCPs according to E_C gives the smallest (average for winter and summer) standard deviation of points from the fit line. This conclusion is valid for both the linear (Table 1) and exponential fits (Table 3).

5 SuperDARN CPCPs measured simultaneously in both hemispheres

The data presented in Figs. 1 and 2 show differences between the summer and winter CPCPs as observed in one hemisphere. One might think that these differences occur because winter and summer data sets correspond to quite different geophysical conditions; after all, the sets do not overlap. We attempted to build a third data set that would include simultaneous SuperDARN CPCP measurements in both hemispheres. Unfortunately, the SuperDARN radar coverage in the Southern Hemisphere is not as good as it is in the Northern Hemisphere. The situation is especially poor for observations during southern summer. The new data set was obtained by considering all events from the northern-summer set that would have reasonable coverage in the southern-winter hemisphere. We required that the amount of points was at least 300 for both hemispheres. This criterion is not easy to achieve for the Southern Hemisphere measurements and, for some convection maps, the foci of only one convection cell was covered by radar measurements. 143 common CPCP measurements were found.

Figure 3 is a scatter plot of the Northern (summer) Hemisphere CPCP versus the southern (winter) CPCP. An upward shift of the cloud of points is obvious indicating that the summer CPCPs are generally larger than the winter CPCPs. This result is consistent with observations in one hemisphere. Unfortunately, there are no points for large CPCPs so that one cannot say in which hemisphere the “saturated” level of the CPCP is larger. More work is needed to isolate events with good coverage in both hemispheres and large CPCP in at least one of these. This is a completely different approach to data selection and we leave the task for future work.

6 Discussion

In this study we plotted the SuperDARN CPCP versus four parameters characterizing the solar wind and its coupling

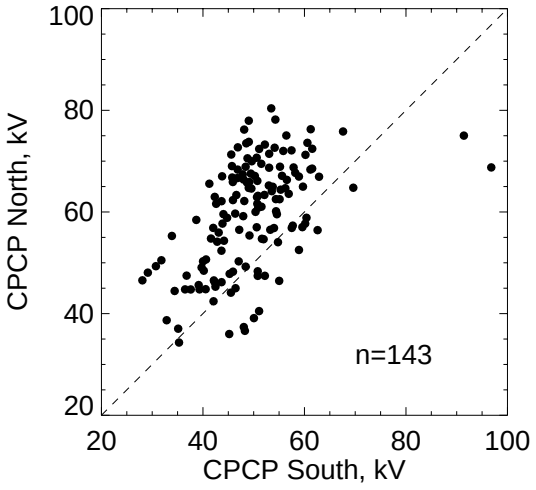

Fig. 3. Scatter plot of SuperDARN CPCP for the Northern (summer) Hemisphere versus SuperDARN CPCP for the Southern (winter) Hemisphere.

with the magnetosphere: IEF, E_{KL}, PCN index and E_C coupling function. We adopted more stringent criteria to individual SuperDARN maps for inferring the CPCP as compared to Khachikjan et al. (2008) matching the approach of Shepherd et al. (2003) who used the E_{KL} coupling function to characterize the SuperDARN CPCP. In contrast to previous studies, we considered summer and winter measurements separately and also considered a limited set of simultaneous observations in both hemispheres.

We note that in addition to investigating the SuperDARN CPCP variation with IEF and E_{KL}(these have been reported in the past) we involved the PCN magnetic index. The objective was that this index is widely used for research in space physics and it would be important to sort out the data according to it. Generally, PCN is considered to be a good proxy for E_{KL} (Troshichev et al., 2006). However, we kept in mind the fact that although correlation between them is high (Troshichev et al., 2006), still these parameters are often not quite the same as evident from Fig. 10 of Troshichev et al. (2006). We should say that the reported SuperDARN CPCPs versus E_{KL} (Fig. 2a, b) are very close to the ones for the PCN index, Fig. 2c, d, but the relationships as assessed by fitting are not quite the same.

Recently, Fiori et al. (2009) presented the SuperDARN CPCPs as a function of PCN, but the data were limited to small PCNs <2 by virtue of considering more recent observations with the Canadian polar cap SuperDARN radar at Rankin Inlet. Results of this paper are only relevant to the linear part of the CPCP-PCN dependence. Importantly, the radar data coverage for the events considered by Fiori et al. (2009) was not as good as in the data sets of the present study. In terms of the variation with the PCN, the present work has a superior SuperDARN data quality and we cover larger range of PCN. It is interesting that despite of different data sets considered, the linear trends reported by Fiori et al. (2009) are consistent with what we present.

All plots of Figs. 1 and 2 show the linear trend at small values of parameters and tendency for the CPCP to saturate at large values. This is very consistent with previous studies that investigated the SuperDARN CPCP relationship with E_{KL} (Shepherd et al., 2003) and IEF (Khachikjan et al., 2008). The linear part of the SuperDARN-based curves for summer is quite consistent with the results of AMIE modeling by Liemohn and Ridley (2002) and Ridley and Khin (2004). Indeed, for the CPCP-IEF dependence, Liemohn and Ridley (2002) reported a slope of 7.29 kV/(mV/m) (for all seasons) while we have 6.26 kV/(mV/m) and 3.65 kV/(mV/m) for summer and winter, respectively, if the linear fitting is applied to entire data set. Such a procedure is probably not good for the winter data. Linear fitting to the growing parts of the scatter plots gives slopes of 8.14 and 11.27 kV/(mV/m), summer and winter, respectively. These numbers are close to the ones of Liemohn and Ridley (2002).

In terms of variation with PCN, Ridley and Kihn (2004) reported the slopes of 16.22 kV/PCN and 15.5 kV/PCN, for summer and winter, respectively. If the CPCP-PCN dependence is simply fit with a straight line, the corresponding slopes for our data would be 10.3 kV/PCN and 5.1 kV/PCN. The smaller slope for the winter data is because the SuperDARN data show clear saturation effect for PCN>4 while the AMIE data do not. The slopes for the "linear" parts of the CPCP-PCN variation for SuperDARN (Table 1) and the AMIE computations of Liemohn and Ridley (2002) do not differ significantly. One also has to note that the Ridley and Kihn (2004) work is limited to PCN<4-5 for winter and <3–4 for summer and this could account for some differences with our results. In terms of the linear slope, the SuperDARN data reported here are also consistent with the satellite-based CPCPs of Troshichev et al. (1996) who reported the value of 19.35 kV/PCN.

For the nonlinear part of the SuperDARN plots consistency with measurements by other techniques is much weaker. Assessment of the SuperDARN data, both visual and with Boltzman and exponential fits (Tables 2 and 3), indicates that the nonlinearity in the dependences starts at relatively small values of the parameters. Visual estimation of the thresholds gives IEF$^*\sim$3 mV/m, PCN$^*\sim$3–4 and $E_C^*\sim 1.5\times 10^4$. These are the numbers that we adopted as the limits of the "linear" domain in the scatter plots. The AMIE modeling shows much larger IEF threshold of $\sim$10 mV/m (Liemohn and Ridley, 2002). Not much of the saturation can be seen for the CPCP-PCN data of Ridley and Kihn (2004). Our plots of the SuperDARN CPCPs versus E_{KL} give the threshold for the nonlinearity of the order of 3 mV/m.

To assess the threshold values for saturation to begin in a more rigorous way, we considered derivative of the Boltzman fit for each data set. Maximum derivative would mean

such a value of the independent variable starting from which the slope of the linear fit line would start to decrease and, eventually, saturation would be achieved. Estimated in this way threshold values for the saturation to begin for summer (winter) are IEF*=1.5 (1.1) mV/m, E^*_{KL}∼1(1) mV/m, PCN*=0 (2.1), and E^*_C=0 (∼6000). We comment that summer variations with PCN and E_C showed declining slopes starting from around zero and, thus, assessing these curves with derivatives is problematic. Obtained threshold values are about 2 times smaller than the ones inferred visually, but they show the same tendencies.

Another issue of the non-linear part of the curves is the level of the CPCP saturation. The data for some plots did not cover the range required to see the saturation confidently, especially for the summer measurements. However, estimates can be inferred from the fits. Tables 2 and 3 indicate that summer parameter A_2 (Boltzman fitting, reflects the saturation level) is larger than the winter one by 9 kV for the IEF plots, and summer parameter P is larger by 1 kV for the PCN plots (exponential fitting), by 23 kV for the E_C plots (exponential fitting), and by 8 kV for the E_{KL} plots (exponential fitting). Larger SuperDARN CPCPs for the summer observations have been mentioned by Shepherd (2007).

To further explore the summer-winter difference in the CPCP of saturation, we selected from our data set a number of events for which reasonable (>300 points) SuperDARN coverage was achieved in the Southern Hemisphere simultaneously with observations in the Northern Hemisphere. We showed (Fig. 3) that the summer (Northern Hemisphere) CPCPs are larger than winter (Southern Hemisphere) ones by ∼10 kV.

Assessment of the SuperDARN CPCP plots by applying various analytical forms of the relationship is not easy because of a significant data spread. We adopted an exponential fit to describe, in relative terms, the change in the parameters from summer to winter and to compare dependencies for IEF, E_{KL}, PCN and E_C. While seasonal changes are mostly discernible for each parameter (such as IEF), inter-comparison of dependencies for the CPCP versus different parameters hardly makes sense, as inferred fit parameters differ significantly.

The SuperDARN CPCPs reported here and elsewhere (e.g., Shepherd et al., 2003; Khachikjan et al., 2008; Fiori et al., 2009) are generally consistent with each other and, in this sense, they represent robustly what the SuperDARN radars are showing on a daily basis. Typical CPCP values of <100 kV are inconsistent with much larger possible values reported in DMSP measurements and AMIE modeling. Figure 7 of Khachikjan et al. (2008) showed that SuperDARN CPCPs begin to divert from AMIE expectations starting from IEF∼5 mV/m. Data by Hairston et al. (2003) from the DMSP satellites show saturation values of ∼150–180 kV. Troshichev et al. (1996) considered EXOS-D satellite measurements of the ion drift for the polar cap crossings and reported essentially a linear CPCP relationship upon the PC index up to ∼5.5 which would roughly correspond to IEF∼5 mV/m.

Differences between CPCPs obtained for similar solar wind conditions but with different techniques is certainly a concern. Unfortunately, the exact reason for this is currently not known; this is an area of active research. For example, Ruohoniemi et al. (2006) selected about 100 DMSP passes over the high-latitude ionosphere for the events with reasonable SuperDARN radar coverage and found that the radars show smaller potentials, although only by ∼15–20%. These were preliminary results and further validation work on the SuperDARN CPCP is ongoing.

As our instrument in this study is the SuperDARN radars, we comment on several aspects of radar measurements that definitively contribute to the CPCP differences, mostly underestimation. Smaller SuperDARN CPCPs as compared to the DMSP measurements is expected because the velocity of F-region echoes at HF tends to be smaller than the $\boldsymbol{E}\times\boldsymbol{B}$ plasma drift component along the beam, as measured by incoherent scatter radars and by ion drift meters on board of DMSP satellites (e.g., Xu et al., 2001; Drayton et al., 2005). The effect is clearly detectable at large drifts of >1 km/s. Xu et al. (2008) statistically compared the DMSP velocity vectors and SuperDARN-inferred convection vectors and showed that the radar velocities are typically smaller than the DMSP ones. Several explanations for the differences have been proposed, including the fact that temporal and spatial resolution of the instruments is not the same. One is a ∼500 km difference in the height of plasma velocity measurements by radars and on satellites. This factor can lead to ∼10% smaller SuperDARN velocities (Sofko and Walker, 2006). The second factor is improper measurement of the Doppler velocity in the routine SD data handling that assumes that the scatter occurs in vacuum. Deviation of the index of refraction from 1 can lead to effective underestimation of the reported SuperDARN velocity by 10–15% (Gillies et al., 2009). If one accepts that the observed SuperDARN velocities are 20% below the $\boldsymbol{E}\times\boldsymbol{B}$ drift magnitude, it would mean underestimation of the electric field by ∼5 mV/m for an average electric field of 25 mV/m. Over a distance of 3000 km, these would lead to the CPCP underestimation by 15 kV. This number doubles for stronger E-field of 50 mV/m. The value of 30 kV is still not enough to explain the differences between SuperDARN and DMSP-based CPCPs.

It is currently believed that as magnetic activity increases, the number of SuperDARN echoes decreases and they tend to be located at short radar ranges. Under these conditions, the SuperDARN CPCP estimates are strongly driven by the startup convection model and, as a result, are somewhat underestimated. For our data set, the typical number of points in individual convection maps was ∼650 for PCN=0-2 and ∼400 for PCN=6–8 for the winter measurements (the number of points for the summer measurements was roughly half of the winter ones). For echoes at short radar ranges, the danger is that they might be coming from the E region.

Several studies showed that the SuperDARN E region velocity is well below the $\boldsymbol{E}\times\boldsymbol{B}$ component along the radar beam (e.g., Makarevitch et al., 2004; Koustov et al., 2005). However, usually, the amount of E-region echoes is not large enough to strongly affect the CPCP estimates. In our analysis, E-region echoes have been excluded from the analysis.

The data presented in Figs. 1–3 show that SuperDARN CPCPs can be significantly larger than the average binned values of ∼80 kV in the saturation regime so that, one might think that, potentially, larger CPCPs are possible if the data search is not limited to cases of large PCN index, one of the main constrains of the present study. To investigate whether this is a correct notion, we processed all SuperDARN 2-min maps for 2002 and inferred maximum CPCP values for each hour irrespective of how many points were available for map processing. In this way, cases with very poor coverage have been considered. We found that although there were cases with CPCP as high as 140 kV, maximum values usually did not exceed 120 kV which we consider as a typical maximum CPCPs that the SuperDARN radars would report. Importantly, these values were achieved for the maps with significant data coverage so that one cannot relate large SuperDARN CPCPs with the startup convection model. In addition, we run the SuperDARN map potential code by considering only the startup convection models (currently, 3 models are implemented). We found that the maximum CPCP values of ∼75 kV are achieved for B_Z^- and B_Y^+ combination. Thus the SuperDARN model CPCPs are significantly smaller than maximum reported values. Clearly, to further clarify the reasons for differences between the SuperDARN CPCPs and measurements/estimates by other methods/techniques, a joint validation work is needed.

7 Conclusions

Results of this study can be summarized as follows. Based on ∼1700 CPCP estimates for summer and ∼1400 CPCP estimates for winter, all in the Northern Hemisphere, we showed that

1. The SuperDARN CPCP shows close-to-linear increase for relatively small values of four parameters widely used to characterize the CPCP: IEF, E_{KL}, PCN index and E_C coupling function of Newell et al. (2007). The linear part of the relationship is consistent with AMIE modeling and satellite measurements. For large values of all these parameters, the SuperDARN CPCP tends to saturate.

2. A transition to the nonlinear regime becomes evident at IEF$^*\sim E_{KL}^*\sim$3 mV/m, PCN* ∼3–4 and $E_C^*\sim 1.5\times10^4$. The threshold values are smaller for winter conditions. Estimated threshold values for the nonlinearity to begin might be affected by the SuperDARN method of the CPCP estimation so that these values can be considered as thresholds starting from which the SuperDARN CPCPs are underestimations of the true CPCP.

3. The SuperDARN CPCP saturation level is slightly (∼1–10 kV) larger for summer conditions. In terms of variation with the IEF, E_{KL}, PCN and E_C, the saturation level is achieved faster during winter; this is a match with smaller winter thresholds for the nonlinearity to kick in. Generally smaller winter CPCPs are also found for limited data set of simultaneous SuperDARN measurements in the summer and winter hemispheres. The average "saturation level" of the SuperDARN CPCP is significantly smaller than the CPCPs reported by other techniques. However, the maximum observed in this study SuperDARN CPCPs of ∼120 kV are typical maximum CPCPs that SuperDARN reported for the entire 2002. The maximum SuperDARN CPCPs are well above the values that the SuperDARN startup convection model would give and they were measured for the maps with good radar coverage.

4. Sorting SuperDARN CPCPs according to the E_C gives the best clustering of the data as evaluated from the standard deviation of the data from the best fit (exponential type) curve.

Acknowledgements. This work was supported by a NSERC (Canada) Discovery Grant to AVK. AVK acknowledges the Institute for Advanced Study, La Trobe University for support during his stay in Australia where he continued work on this project. Critical comments of both reviewers are appreciated.

Topical Editor M. Pinnock thanks O. Troshichev and another anonymous referee for their help in evaluating this paper.

References

Bristow, W. A., Greenwald, R. A., Shepherd, S. G., and Hughes, J. M.: On the observed variability of the cross-polar cap potential, J. Geophys. Res., 109, A02203, doi:10.1029/2003JA010206, 2004.

Drayton, R. A., Koustov, A. V., Hairston, M. R., and Villain, J.-P.: Comparison of DMSP cross-track ion drifts and SuperDARN line-of-sight velocities, Ann. Geophys., 23, 2479–2486, 2005, http://www.ann-geophys.net/23/2479/2005/.

Fiori, R. A. D., Koustov, A. V., Boteler, D., and Makarevich, R. A.: PCN magnetic index and average convection velocity in the polar cap inferred from SuperDARN radar measurements, J. Geophys. Res., 114, A07225, doi:10.1029/2008JA013964, 2009.

Gillies, R. G., Hussey, G. C., Sofko, G. J., McWilliams, K. A., Fiori, R. A. D., Ponomarenko, P., and St.-Maurice, J.-P.: Improvement of SuperDARN velocity measurements by estimating the index of refraction in the scattering region using interferometry, J. Geophys. Res., 114, A07305, doi:10.1029/2008JA013967, 2009.

Hairston, M. R., Hill, T. W., and Heelis, R. A.: Observed saturation of the ionospheric polar cap potential during the 31 March 2001 storm, Geophys. Res. Lett., 30, 1325, doi:10.1029/2002GL015894, 2003.

Khachikjan, G. Ya., Koustov, A. V., and Sofko, G. J.: Dependence of SuperDARN cross polar cap potential upon the solar wind electric field and magnetopause subsolar distance, J. Geophys. Res., 113, A09214, doi:10.1029/2008JA013107, 2008.

Koustov A. V., Sofko, G. J., André, D., Danskin, D. W., and Benkevitch, L. V.: Seasonal variation of HF radar F region echo occurrence in the midnight sector, J. Geophys. Res., 109, A06305, doi:10.1029/2003JA010337, 2004.

Koustov, A. V., Danskin, D. W., Makarevitch, R. A., and Gorin, J. D.: On the relationship between the velocity of E-region HF echoes and $\boldsymbol{E}\times\boldsymbol{B}$ plasma drift, Ann. Geophys., 23, 371–378, 2005, http://www.ann-geophys.net/23/371/2005/.

Liemohn, M. W. and Ridley, A.: Comments on "Nonlinear response of the polar ionosphere to large values of the interplanetary electric field" by C. T. Russell et al., J. Geophys. Res., 107, 1460, doi:10.1029/2002JA009440, 2002.

Makarevitch, R. A., Honary, F., and Koustov, A. V.: Simultaneous HF measurements of E- and F-region Doppler velocities at large flow angles, Ann. Geophys., 22, 1177–1185, 2004, http://www.ann-geophys.net/22/1177/2004/.

Newell, P. T., Sotirelis, T., Liou, K., Meng, C.-I., and Rich, F. J.: A nearly universal solar wind-magnetosphere coupling function inferred from 10 magnetospheric state variables, J. Geophys. Res., 112, A01206, doi:10.1029/2006JA012015, 2007.

Ridley, A. J. and Kihn, E. A.: Polar cap index comparisons with AMIE cross polar cap potential, electric field, and polar cap area, Geophys. Res. Lett., 31, L07801, doi:10.1029/2003GL019113, 2004.

Ruohoniemi, J. M. and Baker, K. B.: Large-scale imaging of high-latitude convection with Super Dual Auroral Radar Network HF radar observations, J. Geophys. Res., 103, 20797–20811, 1998.

Ruohoniemi, J. M., Hairston, M. R., and Shepherd, S. G.: Joint analysis of high-latitude plasma convection with SuperDARN and DMSP, Abstracts of the SuperDARN Workshop 2006, 2006.

Russell, C. T., Luhmann, J. G., and Lu, G.: Nonlinear response of the polar ionosphere to large values of the interplanetary electric field, J. Geophys. Res., 106, 18495–18504, 2001.

Shepherd, S. G.: Polar cap potential saturation: Observations, theory, and modeling, J. Atmos. Terr. Phys., 69, 234–248, 2007.

Shepherd, S. G., Ruohoniemi, J. M., and Greenwald, R. A.: Testing the Hill model of transpolar potential with Super Dual Auroral Radar Network observations, Geophys. Res. Lett., 30, 1002, doi:10.1029/2002GL015426, 2003.

Siscoe, J., Raeder, J., and Ridley, A. J.: Transpolar potential saturation models compared, J. Geophys. Res., 109, A09203, doi:10.1029/2003JA010318, 2004.

Sofko, G. J. and Walker, A. D. M.: Mapping of steady state electric fields and convective drifts in realistic magnetic field models, paper presented at SuperDARN Workshop, Johns Hopkins Univ. Appl. Phys. Lab., Chincoteague, VA, 5–9 June, 2006.

Troshichev, O. A., Hayakawa, H., Matsuoka, T., and Tsuruda, K.: Cross polar cap diameter and voltage as a function of PC index and interplanetary quantities, J. Geophys. Res., 1010(A6), 13429–13435, 1996.

Troshichev, O. A., Janzhura, A., and Stauning, P.: Unified PCN and PCS indices: Method of calculation, physical sense, and dependence on the IMF azimuthal and northward components, J. Geophys. Res., 111, A05208, doi:10.1029/2005JA011402, 2006.

Weimer, D. R., Ober, D. M., Maynard, N. C., Collier, M. R., McComas, D. J., Ness, N. F., Smith, C. W., and Watermann, J.: Predicting interplanetary magnetic field (IMF) propagation delay times using the minimum variance technique, J. Geophys. Res., 108, 1026, doi:10.1029/2002JA009405, 2003.

Xu, L., Koustov, A. V., Thayer, J., and McCready, M. A.: SuperDARN convection and Sondrestrom plasma drift, Ann. Geophys., 19, 749–759, 2001, http://www.ann-geophys.net/19/749/2001/.

Xu, L., Koustov, A. V., Xu, J.-S., Huo, L., and Drayton, R. A.: A 2-D comparison of ionospheric convection derived from SuperDARN and DMSP measurements, Adv. Space Res., 42, 1259–1266, 2008.